

# Growth and Characterization of Nanostructures of III-V Compound Semiconductors

A. G. de Oliveira

Departamento de Física, Instituto de Ciências Exatas, Universidade Federal de Minas Gerais  
Caixa Postal 702, 30161-970 Belo Horizonte, MG, Brasil

Received July 12; revised manuscript received October 25, 1993

In this paper we present a review of the fundamental aspects of Molecular Beam Epitaxy (MBE) applied to III-V compound semiconductors. We start with the basic concept of MBE, then we discuss the *in-situ* technique of RHEED and it is illustrated how the RHEED technique can be used to study both the surface reconstruction and the dynamics of film growth through RHEED intensity oscillations. We will then discuss the doping correlated problems using silicon as the doping element for AlGaAs. Finally, we discuss the persistent photoconductivity (PPC) effect, which is related to the specific defect known as DX center. Both positive and negative PPC are observed and discussed for silicon planar-doped GaAs.

## I. Introduction

In this paper we will review the fundamental aspects of Molecular Beam Epitaxy (MBE), which is a refined form of ultra-high vacuum (UHV) evaporation. The molecular beams are produced by evaporation or sublimation of sources contained in separate crucibles. We will use mostly examples from the AlGaAs alloy system. We will also discuss the *in-situ* technique of reflection high energy electron diffraction (RHEED) known as a powerful technique to study surface reconstructions. One of the features of the surface reconstructions of III-V compound semiconductors is the very wide range of stoichiometry related periodicities. Our approach is based on the concept that most of the surfaces are composed of domain structures rather than precise periodicities. RHEED can also be used to study the dynamics of film growth through the so-called intensity oscillations, which can be used to measure the growth rate *in-situ*. The effective incorporation of both groups III and V species in InAs and InSb during growth were determined and it became clear that the group III rate was dependent on the group V species involved, even at low temperatures. It is shown that controlling the In/Sb flux ratio provides a reliable method of growing cali-

brated InAsSb alloy coinpositions. We will then discuss the doping correlated problems using silicon as the doping element in AlGaAs alloy samples. A strict control of the doping concentrations is basic in the full range of doping concentrations. We will start discussing the conventional and so-called one to one correspondence regime, when every doping atom produces only a specific kind of defect which in turn produces predictable and uniform material properties. In the upper limit the doping element incorporates in different crystallographic sites giving origin to a multiplicity of defects. In this case it is usually quite difficult to predict and control the material properties. Our approach consists first in studying uniformly doped bulk samples and second in studying planar doping structures where diffusion and segregation make the analysis even more complex. The best known and studied simple defects are silicon incorporated on group III and group V element sublattices and the DX center. The complex defects are silicon on one of the sublattices bounded to an intrinsic defect and finally two silicon atoms incorporated on both groups III and V nearest neighbor sublattices. Finally, we discuss the basic concepts of the persistent photoconductivity (PPC) effect. It is generally accepted that the presence of the DX center in silicon doped AlGaAs

alloys with an energy level below the conduction band minimum produces the positive PPC effect that is characterized by the increase of the free-carrier concentration after illumination and by having a nonexponential relaxation behavior after the illumination is turned off. Both positive and negative PPC are being observed on silicon planar doping GaAs samples, which fact in this case makes difficult to establish any simple correlation between DX center and PPC.

## II. Basic technology of molecular beam epitaxy

Demands of progressively thinner planar epitaxial structures have stimulated research into the crystal growth technique known as Molecular Beam Epitaxy (MBE). This is establishing itself as a crystal growth technique with great potential for the fabrication of microwave and optoelectronic devices aiming finally the optical integrated circuits. This is connected with the fact that the MBE technique enables one to tailor the electronic properties of the crystal to the desired function, what has conducted to the introduction of even some until now unknown electronic and structural features. Therefore, a high number of novel semiconductor structures prepared by MBE have been produced having details in the growth direction in the order of only a few lattice parameters.

The simplest way to define the technique of MBE is by considering it as a refined form of vacuum evaporation. The conventional MBE equipment uses materials in liquid or solid forms as sources to produce the molecular beams. Variation of the conventional equipment is the one using gas source in different forms but in the present work we will not discuss such variations. The basic MBE process achieves epitaxial growth over a conveniently heated single crystal substrate in an ultra high vacuum (UHV) environment. The UHV environment is demanded to maintain the unwanted residual impurities as low as possible and to ensure that no gas reaction occurs before the molecules reach the

substrate where the epitaxial growth is determined by complex kinetic reaction processes. This UHV environment is an advantageous feature of MBE because *in situ* surface analytical studies can be carried out in real time just before, during and after the growth, providing therefore a high degree of growth control. The most valuable technique for *in situ* investigation during MBE growth is the reflection high energy electron diffraction (RHEED) which is used a) to determine when native oxides have been removed before growth, b) to determine the growth temperature, c) to study the surface reconstructions, d) to determine precisely the growth rate and e) to study the growth dynamics. A quadrupole mass spectrometer is useful to control the UHV conditions by checking if the concentrations of residual impurities are low enough to obtain good quality samples and to monitor the species emerging from the molecular beam sources. An ion gauge placed in the sample position permits to measure the background pressure and also to monitor the beam fluxes.

The MBE process is illustrated schematically in Fig. 1 that shows five cells, usually referred to as Knudsen cells, which contain crucibles made from pyrolytic Boron Nitride (PBN) with the elements necessary to grow n-doped (Si) and p-doped (Re) AlGaAs. The temperature of each cell is chosen to obtain beams with different fluxes so that the desired chemical composition and doping level can be obtained.

Individual shutters permit to initiate and interrupt each flux independently so that abrupt changes in composition and doping level can be obtained. At temperatures at which the epitaxial layer growths, in a simplified description, the growth rate is determined by the impinging rate of group III elements (Al, Ga) since only those group V atoms (As) necessary to bound the group III orbitals at the surface will be adsorbed. Because of this, the epitaxial growth usually occurs when there are more group V atoms than group III atoms, i.e., in the so-called group V rich conditions. Group III rich conditions are difficult to study because any excess

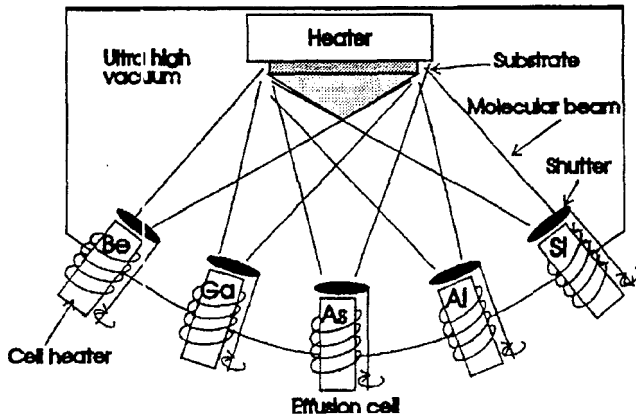


Figure 1: Schematic illustration of a system configuration for growth of doped AlGaAs by MBE. Silicon functions as a donor impurity (n-type dopant) and beryllium functions as an acceptor impurity (p-type dopant).

of group III atoms tends to form free metallic clusters. Typical growth rate range from 0.1 monolayer per second (MLS) to 10 MLS so that usual structures can be modulated in monolayers because the shutter operation times are less than 0.1s. Practical problems come from the need to open and close the shutter many times to produce, e.g., superlattice samples and to raise and lower the temperature of the cells. They were solved by using a microcomputer to control the experience.

To obtain the desired structure with good electrical and optical quality it is necessary to heat the single crystal substrate to temperature ranging from about 400 to 700°C. This is achieved using a heater element inside the growth chamber that can be controlled externally to obtain optimal conditions for temperature, position and rotation. Usually the single crystal substrate is fixed in a molybdenum block that can be coupled to the heater element. At these quite low growth temperatures, one has a non-equilibrium growth ensuring that the reaction on the substrate is strongly moved towards the solidification process. Because of the very low temperatures at which the growth is carried out the diffusion processes in very high composition and doping gradient can be hindered and also the concentration of high temperature thermodynamic defects can be reduced significantly. Another distinguishing characteristics of the MBE growth is that it is possible to

achieve conditions to obtain the so-called layer-by-layer growth mode when the growing interface, improving itself slowly during growth, is atomically smooth. It has been proposed that a step propagation growth mechanism is responsible for this effect<sup>[1]</sup>. Therefore the MBE process permits to obtain the desired hyperabrupt profiles, either in composition and doping, a fact which has been demonstrated by the growth of superlattice, e.g., of thousands of alternating AlAs and GaAs layers, each of them with few monolayers.

Most of the applications in the near future do not require optical or speed capabilities of AlGaAs but new devices that are not possible with silicon are pushing the frontier toward maximum speed in microelectronic devices. Perhaps the most remarkable example of the desire to advance beyond the speed limitations of silicon is related to the concept of MODFET (modulation-doped-field-effect-transistor). The guideline to achieve the unusually high mobilities has been found<sup>[2]</sup> in the study of two-dimensional-electron-gas (2DEG) which can be obtained, e.g., in the band discontinuity between two different materials like in the heterojunction of GaAs/AlGaAs. Electrons from a silicon doped AlGaAs move into the undoped GaAs layer, where the absence of ionised impurities allows the electrons to achieve the high mobilities. An undoped spacer AlGaAs layer, grown between the undoped GaAs layer and the doped AlGaAs layer, is the key factor in improving the mobility for at least a factor of 100<sup>[3]</sup>. The mobility dependence as a function of the spacer layer thickness is shown in Fig. 2. For narrow spacers, the mobility will be determined by the Coulomb scattering of the positively charged parent donor ions near the interface while the decrease in the mobility values for spacer wider than about 800Å is associated with the background impurities in GaAs.

### III. Surface reconstructions

During the last decades considerable insight has been achieved into the surface studies both theoretically

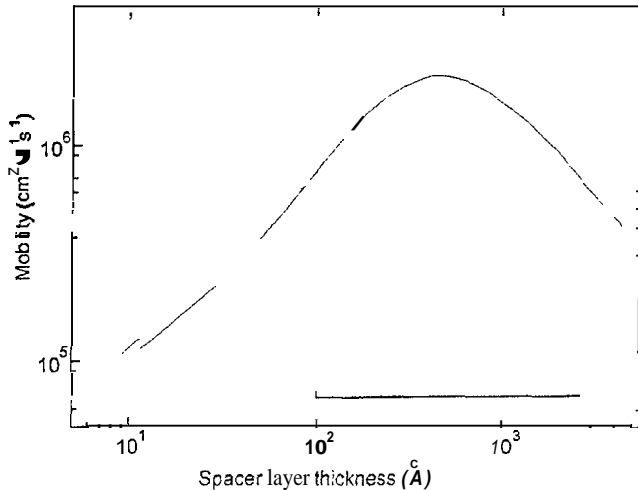


Figure 2: Effect of undoped spacer layer thickness on the mobility of 2DEG structures<sup>[3]</sup>. The inset shows the conduction band structure of a normal version of a MODFET.

and experimentally. With the advent of the Scanning Tunneling Microscopy (STM) technique, direct features of the surface have been seen.

Surface features are intrinsically important to understand the growth mechanism and ultimately to determine the structure properties. Here we will only consider the polar (001) surface on both GaAs and InSb compounds. This surface is ideally terminated by complete monolayer (ML) of either the group III or the group V element, and in general it reconstructs itself. We will focus on the nature and origin of the surface reconstruction and discuss the question of why should the surface reconstruct. The reconstruction usually occurs changing the ideally simple terminated surface of the bulk lattice symmetry to a lower two dimensional symmetry. The form of the reconstruction is related to surface stoichiometry and how specific is this relationship is the important question. The ideal bulk crystal is terminated by two disrupted  $sp_3$  lobes per surface atom, which for the As(Sb)-terminated surface are in the  $[\bar{1}10]$  direction. To reduce the surface energy, dehybridisation occurs creating the dangling bond ( $sp_z$ ) state and the bridge bond ( $p_x - p_y$ ) state. The bridge bond states produce the formation of As-As(Sb-Sb) dimer bound with the arsenic atoms displacing from the ideal crystallographic position<sup>[4]</sup>. This dimer for-

mation mechanism produces therefore a twofold ( $2 \times 1$ ) periodicity and it is illustrated in Fig. 3 and 4.

For the III-V compound semiconductors there is a very wide range of different reconstructions. These different reconstructions can be placed in order of decreasing group III element surface concentration. For GaAs and InSb some of them are respectively:  $c(8 \times 2)-(4 \times 2)$ ,  $(3 \times 1)$ ,  $c(4 \times 6)$ ,  $c(2 \times 8)-(2 \times 4)$  and  $c(4 \times 4)$ ;  $c(8 \times 2)-(4 \times 2)$ ,  $(4 \times 3)$ ,  $a(1 \times 3)$ ,  $c(4 \times 4)$ ,  $(1 \times 3)$ ,  $(7 \times 5)$  and  $(1 \times 1)$ . The symbol  $(n \times m)$  stands for a reconstructed surface having a unit cell  $n \times m$  times larger than the bulk unit cell in real space. The lattice constant is  $n$  times larger in one of the crystallographic direction and  $m$  times in the second direction. The symbol "c" stands for a centered unit cell and "a" stands for asymmetric, as it will be discussed below. More about notation for surface reconstructions can be seen in the work by Wood<sup>[5]</sup>.

The  $c(2 \times 8)$  reconstruction arises from an irregular phasing of dimers along the  $[110]$  direction in adjacent  $(2 \times 4)$  unit cells<sup>[6]</sup>. Both  $c(2 \times 8)$  and  $(2 \times 4)$  reconstructions are present simultaneously so they will not be distinguished in the present work.

Crystallographic models have been formulated for only a few of the observed reconstructions. The group V rich  $(2 \times 4)$  reconstruction is perhaps the best known and it will be considered first. Surface crystallography is most appropriately monitored by RHEED since in this technique the electron beam is at extreme grazing incidence, whereas the molecular beams impinge almost normally on the substrate. The  $(2 \times 4)$  symmetry is promptly obtained from the RHEED technique by real-time observation of the diffraction patterns along two orthogonal  $[110]$  azimuthal directions. In one of the azimuthal direction the diffraction pattern shows one extra diffraction streak, the  $1/2$ -fractional order streak related to the twofold periodicity, between each pair of nearest bulk streaks and in the other azimuthal direction it shows three new extra streaks, the  $1/4$ ,  $2/4$

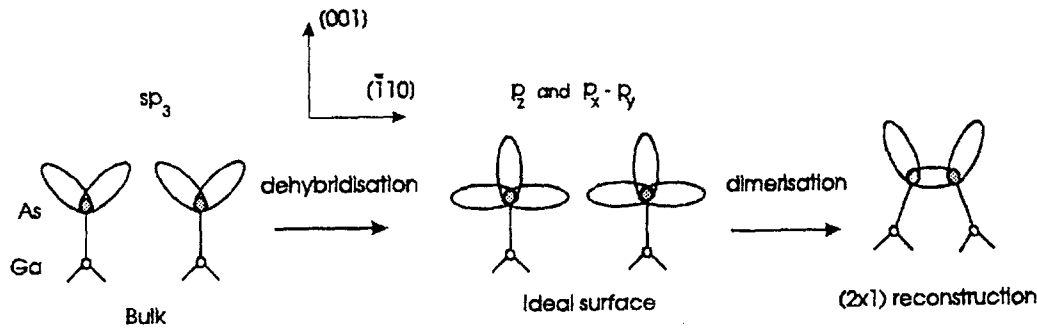


Figure 3: Schematic diagram of the evolution of two newly created disrupted  $sp_3$  lobes to achieve the  $(2 \times 1)$  reconstruction.

and 3/4-fractional order streaks related to the fourfold periodicity. The favoured explanation for the twofold periodicity is the dimerization of arsenic in the  $[\bar{1}10]$  direction. Two different arrangements of dimers have been proposed to account for the fourfold periodicity observed in the orthogonal direction. They are based on STM observations and it is a vacancy model<sup>[7]</sup>, in which the outmost layer coverage is either 0.75 or 0.50 As(Sb)-ML. The former results if every fourth dimer row is missing, whilst the latter comes about from two adjacent missing rows in every four and they are illustrated in Fig. 5. We believe that the  $(2 \times 4)$  reconstruction must be an intrinsic reconstruction because the twofold periodicity is based on the fundamental process of dimerization and the fourfold periodicity comes from the missing row dimer model.

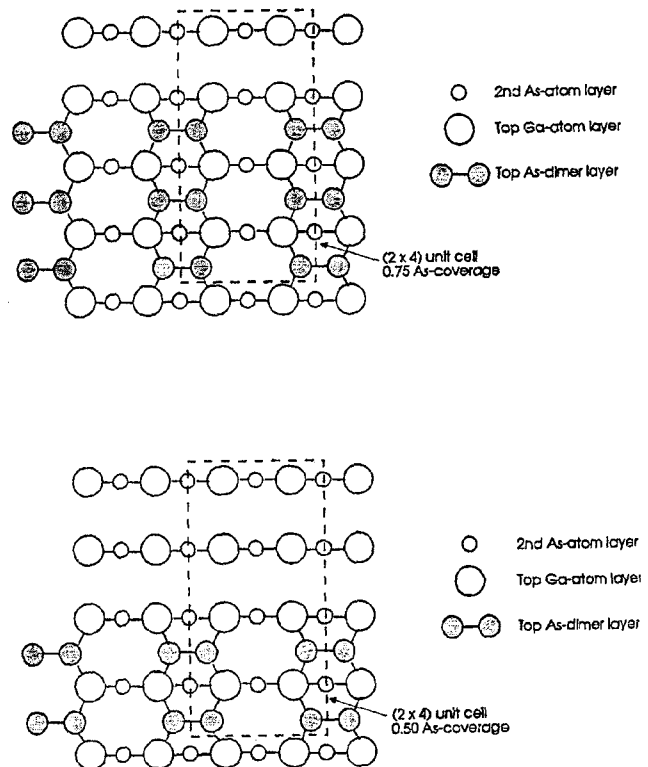


Figure 5: Possible models for de  $(2 \times 4)$  surface reconstruction based on the suppositions of planar dimerisation and of missing row dimers.

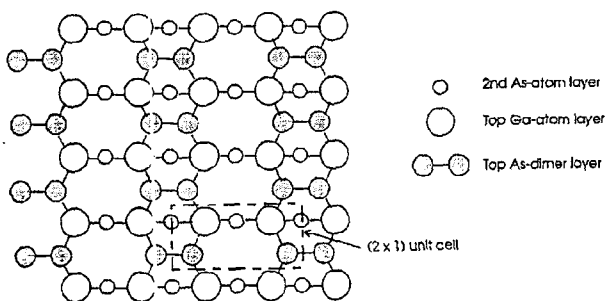


Figure 4: Possible model for the  $(2 \times 1)$  surface reconstruction based on the planar dimerisation.

Our approach hereafter is based on the concept that the wide numbers of surface reconstructions are not intrinsic with precise periodicity but composed of domain structures, which are very much larger than the bulk lattice spacing. We invoke the presence of the complex asymmetric  $a(1 \times 3)$  reconstruction of InSb to support this supposition. The term asymmetric characterises the unequal spacing between the 1/3 and 2/3-fractional order diffraction streaks, defined as the splitting fraction  $F$ . We propose<sup>[8]</sup> a simple model supported by theoretical and experimental evidence to show how

the  $a(1 \times 3)$  structure can be generated from the  $(2 \times 4)$  structure by domain formation invoking the sequencing of the two unit cells with 0.75 and 0.50 ML coverage. To the former we assign the letter A and to the latter, B, to use a convenient shorthand notation. The main clues to understanding the model are the asymmetry and the continuous decrease in  $F$  with decreasing Sb coverage. The superstructure, producing the splitting of the diffraction streaks, would then be generated by introducing a B unit cell in every  $n$  unit cells of the A sequence, creating then a domain length which is  $(n+1)$  times larger than the A or B unit cell. In the most general case the fourfold periodicity is broken to generate an asymmetric sevenfold periodicity. However fivefold and threefold periodicity can be formed depending on whether the  $2/4$ -fractional order streak or both  $1/4$ - and  $3/4$ -fractional streaks have been extinguished respectively. The assumption of the irregular phasing of dimers along the  $[110]$  directions tends to extinguish the half order streak. The formation of the superstructure can therefore be used to explain the  $a(1 \times 3)$  reconstruction. Concluding, we believe that most of the reconstructions for the III-V systems can be explained by domain formation using the  $(2 \times 4)$  unit cell.

#### IV. RHEED intensity oscillations

Reflection high energy electron diffraction (RHEED) has proved to be versatile in its applications for the in-situ investigation of MRE growth dynamics including the effective incorporation rates of both cation and anion species. This was made possible by the introduction of the RHEED intensity oscillation technique<sup>[9]</sup>, which occurs immediately following the start of growth.

Common to the until now proposed models to explain the intensity oscillation is that this occurs due to surface topography changes associated with the layer-by-layer growth mode, i.e., a two-dimensional growth. To understand better this concept it is necessary to establish the nature of the dynamic diffraction processes

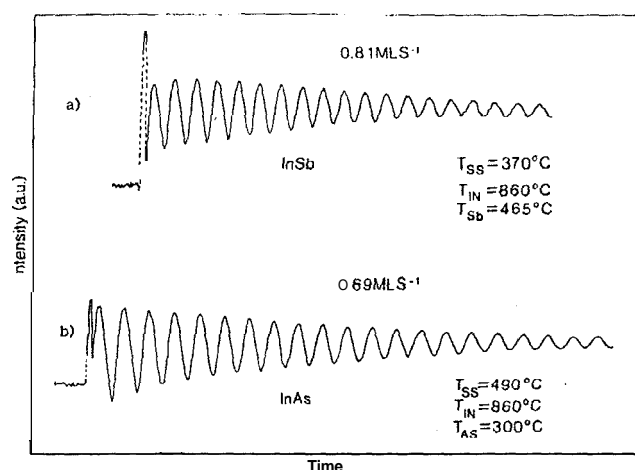


Figure 6: Specular beam intensity trace under equivalent growth conditions for InSb and InAs.

what will not be considered in this lecture. We will consider only the RHEED intensity oscillation to achieve the precise way to measure the effective incorporation rate of elements. A typical data set for the growth of both InAs(001) and InSb(001) layers is shown in Fig. 6 taken using the specular spot on the (00) diffraction streak and with an over-pressure of group V element<sup>[10]</sup>. The steady state period corresponds precisely to the growth of a single monolayer (ML), equivalent to a half lattice parameter. For cations the effective incorporation rate is equated to the absolute growth rate, usually measured in ML per second ( $\text{MLS}^{-1}$ ), and it is supposed to correspond to the group III element flux since its sticking coefficient is admitted to be unity.

Conversely, the sticking coefficient of the anion is seldom unity so that a different procedure is used to calibrate the effective incorporation rate of group V element. The most common procedure<sup>[11]</sup> is using a known excess of the group III element deposited on the substrate surface, with no anion flux present. The excess is typically an amount to grow 10MLs. Higher amounts appear to be detrimental to the surface. In the present example the excess leads to the formation of isolated islands of indium. Intensity oscillations are then induced by opening the shutter of the group V element. The oscillations continue until all of indium excess has been consumed. This model is fully consistent with the

simple group III surface droplet model first proposed by Neave et al.<sup>[11]</sup>. In this model, when the group III element is either predeposited on the substrate surface or supplied in excess over the group V element, clusters are formed on the surface. These clusters then act as sources for group III single adatoms, which react with the group V molecules to form the III-V compound. The oscillation period corresponds to the group V element incorporation rate, which is not equated to the flux, but will be proportional to it. Typical results for the calibration of the antimony flux to grow InSb is shown in Fig. 7. It was observed that for a constant antimony cell temperature there is a negligible effect of substrate temperature on the Sb<sub>4</sub> incorporation rate over the range of typical growth temperature. The calibration of the effective incorporation rate is usually shown in the form of Arrhenius plots. Although the described procedure is a fast and accurate technique for calibrating group V element incorporation rates, it is important to realize that it is not absolute, but is entirely cell-dependent. An alternative condition for observing antimony induced oscillations is growth under indium rich conditions<sup>[10]</sup>.

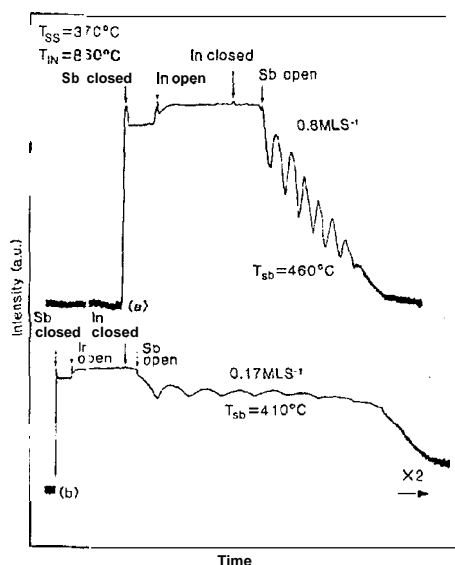


Figure 7: Antimony tetramer induced oscillations observed after deposition of indium on InSb(001). Traces were obtained under the same growth conditions but different antimony cell temperatures.

The above described procedure to calibrate the ef-

fective incorporation rate of group V element helps but it is not an absolute method in determining the alloy composition having two different group V elements, i.e.,  $A_{III}B_V C_V$ . In fact, the determination of the alloy composition using RHEED intensity oscillations can be complicated as illustrated, for example, in the InAsSb system<sup>[10]</sup>.

Conversely, since the sticking coefficient of all group III element is admitted to be unity, the composition of an alloy having two different group III elements, i.e.,  $A_{III}B_V C_V$ , can be directly and precisely evaluated. This supposition is considered to be a very good approximation, but some refinements should be considered if high quality structures are being prepared. We will illustrate this by showing that the effective group III incorporation rate depends on the group V element by comparing the results of RHEED intensity oscillations for the two compounds InSb and InAs. We have shown that for group III element-rich conditions the growth rate observed is due to the group V element availability and for group V element-rich conditions the growth rate observed is due to the group III element availability. Using RHEED intensity oscillations the growth rate of InAs and InSb can be compared to study the influence of the group V element. Fig. 6 shows typical indium-induced oscillations obtained for InSb and InAs.

From these results it is apparent that for a constant indium flux the InSb growth rate is approximately 18% greater than that of InAs for group V element-rich conditions. This difference does not depend on substrate temperature over the range for which oscillations are observed, 250-500°C for InAs and 270-430°C for InSb, and appears to be independent of the magnitude of the anion flux. Correcting the InSb growth rate for the difference in the InSb lattice parameter compared to InAs,  $(6.4794/6.0583)^2$ , still leads to an InSb growth rate that is about 4% higher than that for InAs. We are therefore able to conclude that the effective incorporation of indium depends on the group V element,

and in the case of InAs less than 100% of the indium flux is incorporated under all growth conditions used suggesting that the indium sticking coefficient may be less than unity. The same may be true for InSb, but we could only measure relative values in this context.

The result that, under group V element stable conditions, the effective incorporation rate of indium is dependent on the specific group V element is surprising. Even if we assume that for InSb all of the indium flux is being incorporated as InSb, we must still conclude for InAs that a small fraction of the incident indium is not being incorporated. The fact that the bond strength of In-Sb is higher than In-As may account for a difference between the two compounds, but it does not explain the rejection mechanism. It appears probable that even under group V element rich conditions there may be an accumulation of free elemental indium on the growing surface of InAs, possibly in the form of a moderate density of small clusters. But even this is not a complete explanation because the difference between the total indium flux arriving at the surface and that being incorporated in InAs is too great to be accommodated by surface accumulation alone. Therefore, desorption appears to be the most likely mechanism for the loss of indium.

## V. Dopant incorporation

Nominally undoped GaAs layers grown by MBE using elemental sources are generally found to be p-type with a hole concentration ranging from  $5 \times 10^{14}$  to  $1 \times 10^{15} \text{ cm}^{-3}$ . The main residual p-type impurity in MBE grown samples is carbon, which is identified using photoluminescence spectra. It shows the presence of a shallow acceptor with energy of 26meV at low temperatures.

The incorporation of intentional amount of impurities is achieved by using additional cells. The choice of suitable p- and n-type dopants is of fundamental importance to produce devices. A very great number of elements has been used as doping element for III-

V compounds, e.g., Be, Si, Ge, Sn, S, Se, Te, Cr, Cd and Zn. For alloys in the AlGaAs system, beryllium seems to be an almost ideal p-type dopant and silicon is a near ideal n-dopant and is widely used. Silicon has a unity sticking coefficient, does not exhibit a segregation problem and is relatively insensitive to changes in growth conditions. The silicon doped layers show good electrical and optical properties.

The silicon doped GaAs layers have been intensively investigated over a wide range of doping concentrations. For standard MBE grown samples, with doping concentration below about  $7 \times 10^{18} \text{ cm}^{-3}$ , the carrier concentration is proportional to the silicon flux, indicating that basically all silicon atoms incorporate as donors in the gallium lattice site. This is the so-called one to one correspondence regime when every doping atom produces only a specific kind of defect which in turn produces predictable and uniform material properties. Beyond the one to one correspondence upper limit value the doping element incorporates in different crystallographic sites giving origin to a multiplicity of defects, when then it will be quite difficult to predict and control the material properties. The best known and studied simple defects are produced when silicon atoms incorporate on gallium or on arsenic sublattices. The best known complex defects are produced when silicon atoms incorporate on one of the gallium or arsenic sublattices and are bounded to an intrinsic defect or when two silicon atoms incorporate on both gallium and arsenic nearest neighbor sublattice sites. For alloy samples in the AlGaAs system having an aluminum content higher than about 22%, another simple defect, the so-called DX-center, must also be considered. We show how this multiplicity of defects can be handled studying on heavily silicon doped MBE grown  $\text{Al}_{0.3}\text{Ga}_{0.7}\text{As}$  samples on another work in the present issue<sup>[12]</sup>.

Structures with particular doping profiles can in principle be achieved by monitoring conveniently the temperature of the cells. This is however limited by the time spent to heat up or to cool down the cells.



An alternative way of doping material that permits to overcome this limitation fixed by thermal inertial condition can be obtained by using the planar doping concept<sup>[13]</sup>. Here the dopant is deposited during a growth interruption when the shutters of group III element cells are closed but the shutter of group V element cell is maintained open to ensure the surface stoichiometry. The desired profile is achieved by choosing the appropriated dopant flux and evaporation time. Planar doping has received much interest recently as a method to obtain very high electronic densities, since it seems that compensation mechanisms are reduced when the dopant is introduced in one plane rather than randomly in the bulk. This is reasonable since the number of group III dangling bonds in the surface is minimized during deposition of doping element, therefore reducing their number incorporated on the group V sublattice. This has indeed proved to be correct when, using a comparison of Shubnikov-de Haas measurements and self-consistent numerical calculations, it was shown that a three dimensional equivalent doping level of  $2 \times 10^{19} \text{ cm}^{-3}$  has been achieved<sup>[14]</sup>. Another advantage of this method is that it permits to obtain hyper abrupt doping profile. This is however not ideal because the planar doping profile shows, at high doping levels, the phenomenon of segregation once the solubility limit of doping element on group III sublattice sites is achieved<sup>[15]</sup>. Despite this difficulty the planar doping method can be used to provide good devices. For example, the MODFET structure discussed in the first section can be obtained by replacing the uniformly silicon doped AlGaAs layer by a silicon planar doping structure<sup>[16]</sup>.

## VI. The DX center, the persistent photoconductivity and the planar doping structure

Persistent photoconductivity (PPC) is characterized by the increase of the free-carrier concentration after illumination and by having a nonexponential relaxation behavior after the illumination is turned off. PPC

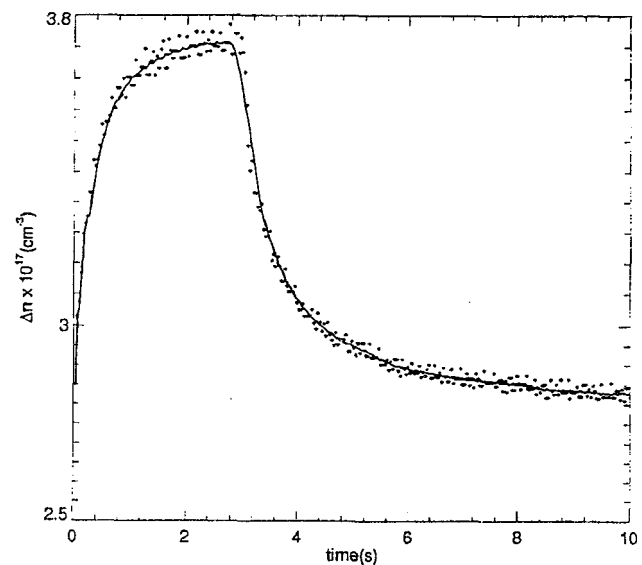


Figure 8: Typical experimental data of the decay of the photoconductivity after the illumination is turned off, as observed in silicon doped AlGaAs layers.

remains for hours or even days after illumination<sup>[17]</sup>. A typical experimental data of the decay of the photoconductivity for silicon doped AlGaAs is shown in Fig. 8.

In spite of the multiple possibility of physical problems that can give origin to PPC, recently PPC is being considered to be the fingerprint of the DX center because it is generally accepted<sup>[18]</sup> that it is responsible for PPC in structures having a silicon doped  $\text{Al}_x\text{Ga}_{1-x}\text{As}$  layer with  $x \geq 0.22$ . It seems now well established that the DX center is an intrinsic feature of n-type dopants and not resulting from complexes related to those impurities. In this view the donor impurity is electronically bistable, having a (fundamental) localized deep (DX) state and a (metastable) extended (d) state.

The most remarkable properties of the DX center are a very large difference (Stokes shift) between its thermal and optical ionization energies and a barrier for electron capture resulting in an exceedingly small electron capture cross section below about 100K<sup>[19]</sup>.

Although the microscopic nature of the DX center is still not completely clear, it is well established that the DX center has a negative charge resulting from the "reaction"  $2d^0 \rightarrow d^+ + DX^-$  where  $d^0$  and  $d^+$  are the neutral and ionized hydrogenic-like shallow donor cen-

ters respectively. Therefore the DX center arises from a substitutional donor by itself and to create one DX center, one  $d^+$  must be destroyed and vice-versa. This has led to suggestions that the DX center involves a displaced donor with lattice relaxations<sup>[19]</sup>.

The reason for the high interest in the PPC effect and its association with the DX center is the detrimental effect it has on device performance, especially at low temperatures. Because of the trend in using planar doping in device fabrication processes, studies involving the correlation between DX center, PPC and planar doping structure assume special relevance. There are, however, no systematic studies done involving the three phenomena. There are only some works reporting the presence of PPC in planar doping structure but in this case it seems to be related to another physical phenomenon, namely a spatial charge separation, instead of the DX center. The first report of negative PPC in planar doping structure is presented somewhere else<sup>[20]</sup>. Negative PPC is characterised by a decrease of the free carrier concentration instead of an increase after illumination. It was suggested that the negative PPC effect is related to the DX center. If that is true, then it will face us with the basic concept of DX center in two dimensions.

### Acknowledgements

I would like to thank my colleagues at the Physics Department for their contributions to the work and FINEP, CNPq, CAPES and FAPEMIG for financial support.

### References

1. A. Y. Cho and J. R. Arthur, *Prog. in Solid State Chem.* **10**, 157 (1975).
2. R. Dingle, H. L. Stromer, A. C. Gossard and W. Wiegmann, *Appl. Phys. Lett.* **33**, 665 (1978).
3. C. T. Foxon and J. J. Harris, *Philips J. Res.* **41**, 313 (1986).
4. J. A. Appelbaum, G. A. Baraff and D. R. Hamann, *Phys. Rev. B* **14**, 1623 (1976).
5. E. A. Wood, *J. Appl. Phys.* **35**, 1306 (1964).
6. B. A. Joyce, J. H. Neave, P. J. Dobson and P. K. Larsen, *Phys. Rev. B* **29**, 814 (1984).
7. M. D. Pashley, K. W. Haberern, W. Friday, J. M. Woodall and P. D. Kirchner, *Phys. Rev. Lett.* **60**, 2176 (1988).
8. A. G. de Oliveira, S. D. Parker, R. Droopad and B. A. Joyce, *Surf. Science* **227**, 150 (1990).
9. J. H. Neave, B. A. Joyce, P. J. Dobson and N. Norton, *Appl. Phys.* **A31**, 1 (1983).
10. I. T. Ferguson, A. G. de Oliveira and B. A. Joyce, *J. Crystal Growth* **121**, 267 (1992).
11. J. H. Neave, B. A. Joyce and P. J. Dobson, *Appl. Phys.* **A34**, 179 (1984).
12. A. G. de Oliveira, G. A. M. Safar and J. F. Sampaio, present issue.
13. C. E. C. Wood, G. Metze, J. Berry and L. F. Eastman, *J. Appl. Phys.* **51**, 383 (1980).
14. R. Rodrigues, P. S. S. Guimaraes, J. F. Sampaio, R. A. Nogueira, A. T. Oliveira Jr., I. F. L. Dias, J. C. Bezerra, A. G. de Oliveira, A. S. Chaves and L. M. R. Scolfaro, *Solid State Comm.* **78**, 793 (1991).
15. J. C. Bezerra, A. G. de Oliveira, M. S. C. Mazzoni and H. Chaciam, present issue.
16. M. V. Baeta Moreira, M. A. Py, M. Gaihanou and M. Ilgeins, *J. Vac. Sci. Technol.* **B10**, 103 (1992).
17. R. J. Nelson, *Appl. Phys. Lett.* **31**, 351 (1977), and references therein.
18. J. F. Sampaio, A. S. Chaves, G. M. Ribeiro, P. S. S. Guimarães, R. P. de Carvalho and A. G. de Oliveira, *Phys. Rev. B* **44**, 10933 (1991).
19. For a recent review, see P. M. Mooney, *J. Appl. Phys.* **67**, R1 (1990).
20. M. I. N da Silva, J. A. Correa F., J. C. Bezerra and A. G. de Oliveira., submitted to *Semicond. Sci. Technol.*